ELSEVIER

CRYOBIOLOGY

Using engineering models to shorten cryoprotectant loading time for the vitrification of articular cartilage

Nadia Shardt [a], Zhirong Chen [a], Shuying Claire Yuan [a], Kezhou Wu [b,d], Leila Laouar [b], Nadr M. Jomha [b], Janet A.W. Elliott [a,c,*]

[a] Department of Chemical and Materials Engineering, University of Alberta, Edmonton, T6G 1H9, Canada
[b] Department of Surgery, University of Alberta, Edmonton, T6G 2B7, Canada
[c] Department of Laboratory Medicine and Pathology, University of Alberta, Edmonton, T6G 2R7, Canada
[d] Department of Orthopedic Surgery, First Affiliated Hospital, Shantou University Medical College, Shantou, Guangdong, China

ARTICLE INFO

ABSTRACT

Osteochondral allograft transplantation can treat full thickness cartilage and bone lesions in the knee and other joints, but the lack of widespread articular cartilage banking limits the quantity of cartilage available for size and contour matching. To address the limited availability of cartilage, vitrification can be used to store harvested joint tissues indefinitely. Our group's reported vitrification protocol [Biomaterials 33 (2012) 6061–6068] takes 9.5 h to load cryoprotectants into intact articular cartilage on bone and achieves high cell viability, but further optimization is needed to shorten this protocol for clinical use. Herein, we use engineering models to calculate the spatial and temporal distributions of cryoprotectant concentration, solution vitrifiability, and freezing point for each step of the 9.5-h protocol. We then incorporate the following major design choices for developing a new shorter protocol: (i) all cryoprotectant loading solution concentrations are reduced, (ii) glycerol is removed as a cryoprotectant, and (iii) an equilibration step is introduced to flatten the final cryoprotectant concentration profiles. We also use a new criterion—the spatially and temporally resolved prediction of solution vitrifiability—to assess whether a protocol will be successful instead of requiring that each cryoprotectant individually reaches a certain concentration. A total cryoprotectant loading time of 7 h is targeted, and our new 7-h protocol is predicted to achieve a level of vitrifiability comparable to the proven 9.5-h protocol throughout the cartilage thickness.

1. Introduction

Damage to articular cartilage in any joint can lead to osteoarthritis, a disease characterized by chronic pain, stiffness, and reduction of mobility [45]. Cartilage is made up of cells known as chondrocytes located within an extracellular collagen matrix that mainly holds proteoglycans and water, and given that it is avascular and aneural, cartilage has a limited ability to repair itself if damaged [31,47]. Focal cartilage lesions can lead to generalized joint deterioration and eventually global osteoarthritis. Prevention of lesion extension is difficult because of the limited ability of cartilage to heal itself. Osteochondral allograft transplantation, where a donor's bone and cartilage is transplanted into a recipient to restore cartilage function, is one established method that can treat small and large cartilage (plus bone) defects [12,14,27,37]. Osteochondral allografting is particularly beneficial for

young patients whose joints are more likely to deteriorate and require a metal joint prosthesis that would not last beyond their lifetime [17,20,28,36,43].

While its clinical success has been demonstrated [12,27,31,37], osteochondral allograft transplantation may not always be possible because of the limited availability of allografts and challenges in size and contour matching [11,14]. Fresh allograft transplantation is logistically challenging because infectious disease testing and precise fitting (for contour, size, and position) has to take place between harvest and transplantation [11,12,15,52], and the additional time needed to perform these steps compromises chondrocyte viability. The timeframe available for testing and matching can be extended by storing allografts at 4 °C, but chondrocyte viability deteriorates after 14 days under hypothermic storage in culture media [7]. A long-term storage technique is needed to maintain cartilage allografts and chondrocyte viability, allow

---

for necessary testing and matching to occur, and facilitate allograft availability for future transplantation.

Vitrification is a promising method for storing cartilage for extended periods of time [3,33,38]. This method consists of loading high concentrations of cryoprotectants into a cell or tissue that depress the freezing point to such an extent that damaging ice formation is avoided while an amorphous solid is formed when the cell or tissue is cooled rapidly enough past its glass transition temperature [56]. Common permeating cryoprotectants used in vitrification include dimethyl sulfoxide (Me$_2$SO), glycerol, ethylene glycol (EG), propylene glycol (PG), and formamide [25,38], and their selection depends on the type of tissue as well as interactions between the cryoprotectant and the tissue. In the design of cryoprotectant loading protocols for vitrification, three important variables need to be quantified: cryoprotectant permeation, vitrifiability, and toxicity [9,22,24,33]. Sufficiently high levels of cryoprotectant permeation [4,34] and cryoprotectant vitrifiability [55] are needed to ensure that an amorphous state is achieved at the cooling rate attainable when a sample is plunged into liquid nitrogen, while sufficiently low levels of cryoprotectant toxicity [19,21,35] are simultaneously needed to avoid damage to the cells from the cryoprotectants themselves. Toxicity can be mitigated by using multiple cryoprotectants instead of a single cryoprotectant at the same total concentration [6,13, 23] and by loading cryoprotectants at lower temperatures because toxicity decreases with temperature [19,40]. These observations about toxicity motivate the design of liquidus tracking methods for loading multiple cryoprotectants in tissue in a step-wise manner for vitrification [3,10,26,46,53,54].

The systematic design of cryoprotectant loading protocols for articular cartilage can be aided by using engineering models of cryoprotectant permeation, vitrifiability, and freezing point of multi-cryoprotectant solutions. Fick's law is an empirical, ideal model of cryoprotectant diffusion that has been used to gain insight into the kinetics of cryoprotectant loading and removal [4,34,41,44,50], but it ignores water movement. Building on the biomechanical triphasic model of articular cartilage developed by Lai et al. [39] and Gu et al. [29], Zhang and Pegg [49] proposed the inclusion of cryoprotectants in the triphasic model, making the simplifying assumptions that the cryoprotectants were ideal and dilute. To account for the actual nonideality of high cryoprotectant concentrations, a modified triphasic model was developed by Abazari et al. [1,5] to predict cryoprotectant permeation and water movement into and out of articular cartilage as a function of time and position in the cartilage. The modified triphasic model was compared to predictions calculated using Fick's law of diffusion in 1-dimension, and it was shown that Fick's law underestimates the predictions of the triphasic model [2]. However, if the cryoprotectant and cartilage properties needed to implement the triphasic model are unknown, Fick's law can be used instead for conservative protocol design [50]. Recently, the 2-dimensional form of Fick's law was used to predict the spatial and temporal distribution of cryoprotectants in human cartilage dowels during loading and efflux experiments, and the equilibrium efflux predictions agreed with experimental measurements within 15% (cryoprotectant diffusion coefficients in porcine cartilage were used as approximations of those in human cartilage) [50]. This agreement is in part due to the fact that effective diffusion coefficients were used, which were obtained by fitting Fick's law to real, nonideal experimental data [4,34]. The toxicity of common cryoprotectants in porcine [19,35] and human [6] articular cartilage has been measured as a function of temperature and time of exposure, and theoretical models have been developed to describe these toxicity trends [19,21,35] and to design toxicity-optimal procedures for loading cryoprotectants using a mathematical toxicity cost function [8]. Weiss et al. used logistic regression to develop a statistical model for predicting the vitrifiability and glass stability of large volume (5 mL) multi-cryoprotectant solutions containing Me$_2$SO, glycerol, PG, EG, and formamide, and the proposed vitrifiability model accurately described all experimentally studied solutions [55]. To design a liquidus tracking protocol, the freezing point of

Table 1
Cryoprotectant concentrations, times, and temperatures for each step of the successful 9.5-h protocol [33].

	Concentrations	Time	Temperature
Step 1	6 M Me$_2$SO	90 min	0 °C
Step 2	2.4375 M Me$_2$SO 6 M glycerol	220 min	0 °C
Step 3	2.4375 M Me$_2$SO 1.625 M glycerol 6 M PG	180 min	−10 °C
Step 4	2.4375 M Me$_2$SO 1.625 M glycerol 0.8125 M PG 6 M EG	80 min	−15 °C

the cryoprotectant solution can be calculated using the multi-solute osmotic virial equation [18,48,58] that accounts for the nonideality of highly concentrated cryoprotectant solutions more accurately than ideal-dilute models [48,58].

By considering the previous work in quantifying cryoprotectant permeation, vitrifiability, and toxicity, a successful 9.5-h loading protocol for dowels of articular cartilage attached to bone reported by Jomha et al. achieved high cell viability after vitrification and warming [33]. Cartilage dowels were placed sequentially in four cryoprotectant solutions containing Me$_2$SO, glycerol, PG, and EG at different concentrations, temperatures, and times of exposure selected to attain a minimum total cryoprotectant concentration of 6.5 M at the bone–cartilage junction necessary for vitrification (see Table 1 for details). To facilitate the implementation of vitrification for the long-term storage of articular cartilage in tissue banks, shortening and optimization of loading protocols is required. Each step of the loading protocol reported in Jomha et al. [33] was modeled using Fick's law to lend insight into the dynamic process of diffusion [50], and it was proposed that the 9.5-h protocol could be completed in 7 h while still attaining the same minimum concentration of each cryoprotectant for a total of 6.5 M in a cartilage sample with 2-mm thickness [50]. In that hypothetical 7-h protocol, three loading steps with the cryoprotectant solutions as listed in steps 2–4 in Table 1 were proposed with times and temperatures of 210 min at 0 °C for step 2, 90 min at −7 °C for step 3, and 120 min at −10 °C for step 4.

The criterion for designing the 9.5-h protocol [33] and the hypothetical 7-h protocol [50] was the attainment of a minimum concentration of each individual cryoprotectant by the end of the loading protocol, but these individual concentrations are, together, only one possible combination out of an infinite number of vitrifiable cryoprotectant concentrations. Additionally, the spatial distribution of cryoprotectant concentration was not uniform throughout the cartilage thickness for these protocols, with unnecessarily high concentrations close to the cartilage–solution boundary. In the present study, we instead adopt a new criterion: the predicted vitrifiability of the cryoprotectant solution throughout the cartilage thickness must exceed a certain threshold. This new criterion can be used to screen a greater number of potential cryoprotectant types and concentrations. We also introduce a final equilibration step to create a more uniform spatial distribution of cryoprotectant. Implementing a vitrifiability criterion and an equilibration step allows us to design a new protocol predicted to have lower toxicity.

The objectives of the present work are: (a) to calculate the expected spatial and temporal distribution of vitrifiability for each step of the proven 9.5-h protocol [33]; (b) to design a new 7-h protocol that is predicted to have a similar level of vitrifiability to the 9.5-h protocol while reducing cryoprotectant toxicity; (c) to highlight the importance of correctly accounting for the nonideality and non-dilute nature of vitrifiable cryoprotectant solutions when calculating their freezing points; and (d) using the vitrifiability criterion, to explain why a minimally vitrifiable 5-h protocol reported in the literature was unsuccessful when performed experimentally [57].
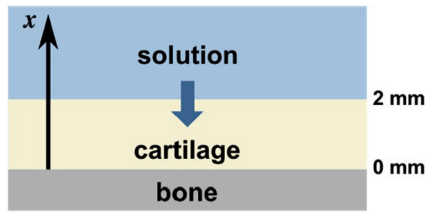
Fig. 1. Schematic of cartilage (thickness = 2 mm) attached to bone in a cryoprotectant solution.

2. Governing equations

Fig. 1 illustrates the slab geometry of cartilage with a thickness of 2 mm attached to bone placed in a cryoprotectant solution. A 2-mm thickness was selected as a representative value of actual human femoral cartilage thicknesses that can range between 1.65 mm and 2.98 mm [50,51]. The surface area of chondral and osteochondral defects can be between 0.5 cm^2 and 12 cm^2 [30], so entire condyles would need to be banked to permit precise sizing and matching when transplantation is needed. For a condyle, the surface area available for diffusion is much greater from the top surface than from the sides. Therefore, for our calculations, we assume that diffusion occurs only in the axial (x) direction so that the designed loading protocol can be used for cartilage covering a whole condyle.

2.1. Permeation

Fick's law of diffusion is used for each cryoprotectant, and for 1-dimensional diffusion it is given by

$$\frac{\partial C}{\partial t} = D \frac{\partial^2 C}{\partial x^2} \tag{1}$$

where C is the molar concentration of the cryoprotectant, x is the axial position in the cartilage, t is the time, and D is the diffusion coefficient of the cryoprotectant given by the Arrhenius expression [4,34]:

$$D = A \exp\left(-\frac{E_a}{RT}\right) \tag{2}$$

where R is the universal gas constant, T is the absolute temperature, A is a prefactor, and E_a is the activation energy. Each cryoprotectant has a different A and E_a when diffusing into articular cartilage, values of which were determined from measurements on porcine articular cartilage and are summarized in Table 2 [4,34]. We note that Fick's law is inherently ideal and cannot directly describe water movement and the associated swelling and shrinking of the articular cartilage. However, when effective diffusion coefficients are determined by fitting to experimental data of actual cryoprotectant diffusion, this fitting empirically captures the net effect of water transport and solution nonideality on the expected cryoprotectant concentration in the cartilage. It was shown by Shardt et al. [50] that empirically-obtained effective porcine diffusion coefficients, when substituted into Fick's law, could be used to approximate diffusion in human articular cartilage dowels. Additionally, the permeation of multiple cryoprotectants could be approximated by separately calculating the permeation of each

Table 2
Coefficients for use in the Arrhenius expression (Equation (2)) [4] of each cryoprotectant considered in the present study.

	A (m^2/s)	E_a (kcal/mol)
Me$_2$SO	2.9895×10^{-7}	3.9 ± 1.6
Glycerol	2.0803×10^{-6}	5.6 ± 1.2
PG	1.6971×10^{-5}	6.63 ± 0.04
EG	1.833×10^{-7}	3.8 ± 0.7

Table 3
Scoring of the ordinal model of vitrifiability [55].

Ordinal Score	Description
0	No vitrification
1	Complete devitrification
2	Partial devitrification
3	Devitrification at edges
4	No devitrification

individual component (interactions between cryoprotectants during diffusion do not seem to be significant).

2.1.1. Initial conditions and boundary conditions

To solve Equation (1), initial and boundary conditions need to be defined. For the first step of a loading protocol (at $t = 0$), there are no cryoprotectants in the cartilage. That is, the initial condition is given by

$$C(0 < x < 2\,\text{mm}, t = 0) = 0 \tag{3}$$

For each subsequent step of the loading protocol, the initial condition for each cryoprotectant is its concentration profile at the end of the previous step.

Two boundary conditions are defined as follows. The first is that the concentration of each cryoprotectant at the solution–cartilage boundary equals that in the surrounding solution and is constant with time in each loading solution:

$$C(x = 2\,\text{mm}, t) = C_{solution} \tag{4}$$

The second boundary condition is at the bone–cartilage boundary where we assume that there is no flow of cryoprotectant. Mathematically, this can be expressed as

$$\frac{\partial C}{\partial x}(x = 0\,\text{mm}, t) = 0 \tag{5}$$

Given these initial and boundary conditions, Equation (1) is solved using the built-in partial differential equation solver *pdepe()* in Matlab 2018a (Natick, MA, USA).

2.2. Vitrifiability

Based on the concentration distribution calculated by Fick's law, predictions of vitrifiability can be calculated as a function of axial

Table 4
Thresholds (α) and coefficients (β) for the ordinal model of vitrifiability [55].

Parameter	Estimate
α_1	167.6 ± 29.2
α_2	184.0 ± 31.5
α_3	186.8 ± 31.8
α_4	190.5 ± 32.0
β_{PG}	57.1 ± 10.6
β_{Glyc}	45.9 ± 8.6
β_{EG}	39.9 ± 8.0
β_{Me_2SO}	36.4 ± 6.7
β_{PG_Glyc}	-7.0 ± 1.4
β_{PG_EG}	-5.9 ± 1.3
$\beta_{Me_2SO\_PG}$	-5.9 ± 1.2
β_{EG_Glyc}	-5.0 ± 1.1
$\beta_{Me_2SO\_Glyc}$	-4.3 ± 0.9
β_{PG_PG}	-4.1 ± 0.9
$\beta_{Me_2SO\_EG}$	-3.7 ± 0.9
β_{Glyc_Glyc}	-2.9 ± 0.7
β_{EG_EG}	-2.3 ± 0.6
$\beta_{Me_2SO\_Me_2SO}$	-1.4 ± 0.4

Table 5
Coefficients for use in the multi-solute osmotic virial equation (Equation (8)) [58] and the molar volume [16] of each cryoprotectant considered in the present study.

	k	B (molal^{-1})	V_m (L/mol)
Me$_2$SO	1	0.108 ± 0.005	0.0709
Glycerol	1	0.023 ± 0.001	0.0731
PG	1	0.039 ± 0.001	0.0735
EG	1	0.020 ± 0.001	0.0559
NaCl	1.678	0.044 ± 0.002	–

position in the cartilage. The vitrifiability of a cryoprotectant solution is not only a function of its composition, but also of its volume and the cooling rate it undergoes. To develop a statistical model for the vitrifiability of solutions at volumes and cooling rates commonly used in vitrification protocols, Weiss et al. [55] prepared 164 different multi-cryoprotectant saline solutions with total cryoprotectant concentrations between 6 M and 9 M, transferred 5 mL of the solutions to 10 mL polypropylene tubes, and plunged the tubes into liquid nitrogen (cooling rate of approximately 60 K/min [32,55]). After 30 min in liquid nitrogen, the solutions were removed, immersed in a water bath at 37 °C until completely liquefied, and an ordinal score to describe vitrifiability and stability was assigned by visual inspection (scores of 0–4 corresponding to a range of outcomes between no vitrification to no devitrification, as described in Table 3).

For the cryoprotectant solutions studied by Weiss et al. [55] to reach a certain ordinal score, the numerical value calculated using the following equation must exceed increasingly higher threshold values α_n (Table 4) [55]:

$$\sum_{i=1}^{p} \left[\beta_i C_i + \sum_{j=1}^{i} \beta_{ij} C_i C_j \right] \geq |\alpha_n| \qquad (6)$$

where β_i is the coefficient for cryoprotectant i, β_{ij} are coefficients of the interaction terms between all combinations of two cryoprotectants (including self-interactions), as summarized in Table 4 [55], C_i is the

molar concentration of cryoprotectant i (mol/L), and p is the number of cryoprotectants present in solution. All coefficients β_i and β_{ij} were calculated using proportional-odds logistic regression applied to the experimentally determined ordinal scores of multi-cryoprotectant solutions, and the listed coefficients are only valid for predicting the vitrifiability of 5 mL solutions in 10 mL polypropylene tubes cooled at ~60 K/min or other solutions under equally, or more, favorable conditions (e.g., smaller volumes or higher cooling rates).
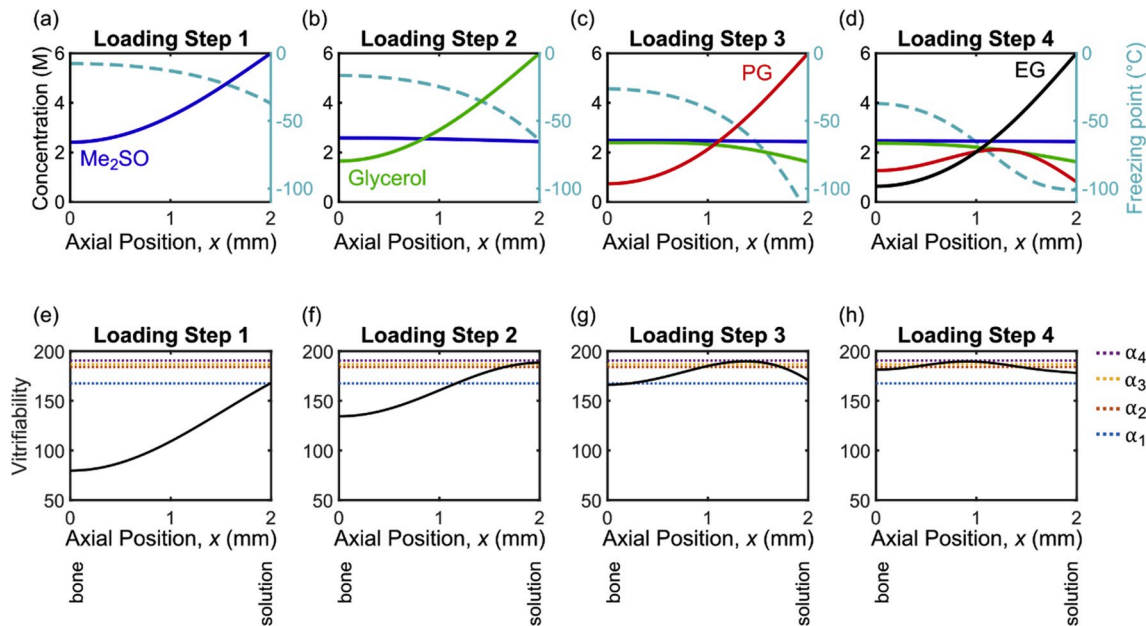
2.3. Freezing point

Given the concentration profiles calculated by Fick's law, we calculate the freezing point at each location throughout the cartilage thickness. The freezing point of an aqueous solution is given by [18,48,58]:

$$T_{FP}^0 - T_{FP} = \frac{\left[W_1 / \left(\overline{s_1^{0L}} - \overline{s_1^{0S}} \right) \right] R T_{FP}^0 \pi}{1 + \left[W_1 / \left(\overline{s_1^{0L}} - \overline{s_1^{0S}} \right) \right] R \pi} \qquad (7)$$

where T_{FP}^0 is the freezing point of water (273.15 K), T_{FP} is the freezing point (K) of the solution with an osmolality of π (osmol/kg solvent), W_1 is the molar mass of water (0.01802 kg/mol), and $\overline{s_1^{0L}} - \overline{s_1^{0S}}$ is the difference between the molar entropy of pure liquid water and of pure solid water at T_{FP}^0 ($\overline{s_1^{0L}} - \overline{s_1^{0S}} = 22.00$ J/mol K). The osmolality of the solution is calculated using the multi-solute osmotic virial equation [18,48] based on the fitting coefficients reported by Zielinski et al. [58] for Me$_2$SO, glycerol, PG, and EG. For these cryoprotectants, the second order virial coefficients are sufficient to accurately calculate osmolality, and the following equation is used to calculate solution osmolality in this study:

$$\pi = \sum_{i=2}^{r} k_i m_i + \sum_{i=2}^{r} \sum_{j=2}^{r} \frac{B_i + B_j}{2} k_i m_i k_j m_j \qquad (8)$$

where m_i is the molality (mol/kg solvent) of the $(i-1)^{\text{th}}$ cryoprotectant, k is the dissociation constant, and B is the second osmotic virial

Fig. 2. (a)–(d) Spatial distribution of cryoprotectant concentration (solid lines; blue is Me$_2$SO, green is glycerol, red is PG, and black is EG; left y-axis) and freezing point (dashed line, light blue; right y-axis) in a 2-mm thick cartilage sample at the end of each step of the 9.5-h loading protocol, the details of which are summarized in Table 1. (e)–(h) Spatial distribution of vitrifiability (black solid line) at the end of each loading step with vitrifiability thresholds illustrated by dotted horizontal lines (blue is α_1, red is α_2, yellow is α_3, and purple is α_4). Concentration is calculated using Equations (1)–(5), freezing point is calculated using the nonideal equations (Equation (7)–(9)), and vitrifiability is calculated using Equation (6). (For interpretation of the references to colour in this figure legend, the reader is referred to the Web version of this article.)

coefficient for each of the $r - 2$ cryoprotectants present in solution, as listed in Table 5 [58]. The summations start from an index of 2 because water is defined as component 1 in Equation (7) by convention. The $(r - 1)^{\text{th}}$ solute in the intracellular solution is NaCl at a molality of $m_{\text{NaCl}} \approx$ 176 mmol/kg (isotonic salt concentration). The molality of each cryoprotectant is determined from its molar concentration using the following equation:

$$m_i = \frac{\left(1000 \frac{\text{L}}{\text{m}^3}\right) C_i}{\rho_1 \left[1 - \sum_{i=2}^{r-1} C_i V_{m,i}\right]} \tag{9}$$

where ρ_1 is the density of water (998 kg/m^3 at 22 °C [42]) and $V_{m,i}$ is the molar volume of each cryoprotectant (L/mol) calculated at 22 °C from the DIPPR 801 database [16], as listed in Table 5. Equation (9) assumes that the volume of mixing is negligible and that the volume of NaCl and other minute additives is negligible compared to the volumes of cryoprotectants and water. Instead of Equation (9), previous work [50] used the conversion $m_i = (1000)C_i/(\rho_1[1 - C_i V_{m,i}])$, which is only accurate for single-solute solutions.

To highlight the importance of using Equations (7)–(9), we also compute the freezing point with the assumption of an ideal-dilute solution. If we make such an incorrect assumption (indicated by * in equations) for a highly-concentrated cryoprotectant solution, the molality of each cryoprotectant is related to the molar concentration by the following expression

$$m_i^* = \left(1000 \frac{\text{L}}{\text{m}^3}\right) \frac{C_i}{\rho_1} \tag{10}$$

The osmolality of an ideal dilute solution is calculated by

$$\pi^* = \sum_{i=2}^{r} m_i = \sum_{i=2}^{r} \left(1000 \frac{\text{L}}{\text{m}^3}\right) \frac{C_i}{\rho_1} \tag{11}$$

and a linearized form of the equation for the freezing point of a cryoprotectant solution is used [48,58]:

$$T_{FP}^0 - T_{FP}^* = 1.86\pi \tag{12}$$

where π is calculated using Equation (11) to yield:

$$T_{FP}^0 - T_{FP}^* = 1.86 \sum_{i=2}^{r} \left(1000 \frac{\text{L}}{\text{m}^3}\right) \frac{C_i}{\rho_1} \tag{13}$$

3. Results and discussion

3.1. Spatial distribution of vitrifiability for the 9.5-h protocol

Fig. 2 illustrates the calculated spatial distribution of cryoprotectant concentration, freezing point, and ordinal vitrifiability at the end of each loading step of the 9.5-h protocol. The solid lines in (a)–(d) illustrate the concentration profiles as calculated by Fick's law (Equation (1) with boundary conditions defined by Equations (4) and (5) and diffusion coefficients from Equation (2) with the Arrhenius parameters listed in Table 2). Based on these concentration profiles, the freezing point at each location in the cartilage thickness is calculated assuming nonideal solution behavior (Equation (7)–(9) with parameters from Table 5), and the spatial distribution of freezing point is plotted with a dashed line for each loading step. The vitrifiability profiles (black lines in (e)–(h)) are calculated using Equation (6) with the coefficients obtained by Weiss et al. [55] listed in Table 4. The dotted horizontal lines in figures (e)–(h) represent the four thresholds (α_i) of increasing ordinal vitrifiability [55]. At the end of the first step, none of the cartilage has reached a vitrifiable cryoprotectant concentration, but by the end of the last step, the level of vitrifiability exceeds the threshold α_1 throughout the thickness of the cartilage.

3.2. Spatial distribution of vitrifiability for the new 7-h protocol

To shorten the 9.5-h protocol and reduce toxicity, we incorporate the following five design choices to create a 7-h protocol with 3 loading steps. First, since the toxicity of cryoprotectants decreases as concentration decreases, each cryoprotectant's concentration in the loading solutions is lowered from 6 M to a maximum of 3 M (cryoprotectant mixtures at a total concentration of 3 M are associated with low toxicity at a temperature of 37 °C [35], and toxicity decreases with temperature, so loading at temperatures near the solution's freezing point will further decrease toxicity). Second, we note that glycerol and PG have similar diffusion rates into articular cartilage, and both diffuse much slower than Me$_2$SO and EG [34]. PG individually contributes more to the vitrifiability of a solution than glycerol (Table 4), so PG is kept as a cryoprotectant and glycerol is removed to help shorten the overall time needed to load cryoprotectants while maintaining high vitrifiability. Glycerol was also found to be the most toxic to full-thickness articular cartilage [21] possibly because of added dehydration stress [5]; thus, removing glycerol will reduce the overall toxicity of the cryoprotectant loading protocol. Third, since Me$_2$SO permeates the fastest, it can be loaded simultaneously with EG in a single step (an approach used by Shardt et al. [50]), and the first loading step of the 9.5-h protocol is removed entirely. Fourth, since PG is more toxic than Me$_2$SO or EG, it should be loaded in the second step at a lower temperature to mitigate its toxicity (made possible by the depression in freezing point from the addition of Me$_2$SO and EG in the first step). Fifth, the purpose of a third loading step is to flatten out the concentration profile of PG so that cells closer to the solution are not exposed to unnecessarily high concentrations of toxic PG during the time needed for rewarming the solution from the temperature of liquid nitrogen. As the PG concentration profile flattens, the concentration of the other cryoprotectants continues to increase as the solution concentration of each other cryoprotectant is maintained at 3 M in this third step. We set the concentration of PG in the third loading step to 2 M and allow some time for equilibration. Taken together, the five design choices above yield the following cryoprotectant concentrations for each loading step: the 1st loading step has 3 M Me$_2$SO and 3 M EG; the 2nd loading step has 3 M Me$_2$SO, 3 M EG, and 3 M PG; and the 3rd loading step has 3 M Me$_2$SO, 3 M EG, and 2 M PG.

The times and temperatures of the 3 loading steps are modified until the following conditions are met for all positions $0 < x < 2$ mm in the cartilage: (a) the vitrifiability as calculated by Equation (6) must exceed at least the threshold α_1, and (b) the temperature of each loading step must be greater than the freezing point as calculated at the end of the previous step. We impose a limit of 7 h on the total time of the loading protocol.

Since just two of the cryoprotectants (Me$_2$SO and EG) are loaded in the first step, the length of this step should only be long enough to allow sufficient permeation for the freezing point at the bone to reach less than -5 °C. A time of 90 min for the first loading step fulfills this requirement. Then, all three cryoprotectants can permeate into the cartilage during the second loading step at a temperature of -5 °C. The freezing point will be depressed further as the concentration of each cryoprotectant increases throughout the cartilage thickness, allowing for the third loading step to take place at -10 °C.

Given a total loading time of 7 h (420 min) and a first loading step time of 90 min, the remaining 330 min can be split between the second and third loading steps. There are two extremes for splitting the 330 min. The longer the second step is, the more cryoprotectant will permeate. Giving a minimum 10 min for the last step, this leaves a time of 320 min for the second step. For these times (90 min; 320 min; 10 min), the minimum ordinal vitrifiability achieved across the 2-mm thickness is at the bone with a value of 179 according to Equation (6). On the other hand, the longer the third step is, the more even the distribution of concentration across the thickness will be. The longest possible time of the third step while still exceeding α_1 is 290 min, leaving

Table 6

Cryoprotectant concentrations, times, and temperatures for each loading step of the new 7-h protocol.

|	Concentrations	Time	Temperature
Step 1	3 M Me₂SO	90 min	0 °C
	3 M EG		
Step 2	3 M Me₂SO	170 min	−5 °C
	3 M EG		
	3 M PG		
Step 3	3 M Me₂SO	160 min	−10 °C
	3 M EG		
	2 M PG		

40 min for the second step. For these times (90 min; 40 min; 290 min), the minimum ordinal vitrifiability is 168. As a compromise between a high vitrifiability and an even distribution of cryoprotectant concentration, we choose times of 90 min for step 1, 170 min for step 2, and 160 min for step 3 to yield a minimum ordinal vitrifiability of 174 at the bone. The concentrations, times, and temperatures of this new 7-h protocol are summarized in Table 6, and Fig. 3 shows the calculated spatial distribution of cryoprotectant concentration (Equation (1)–(5)), freezing point (Equation (7)–(9)), and ordinal vitrifiability (Equation

(6)) at the end of each step of the new 7-h loading protocol.

Along with being 2.5 h shorter than the 9.5-h protocol, we emphasize that the new 7-h protocol is expected to be less toxic compared to the 9.5-h protocol [33] from four perspectives. First, the maximum concentration of any single cryoprotectant is reduced from 6 M to 3 M; second, glycerol is removed; third, the total time of exposure to cryoprotectants is lowered by 2.5 h; and fourth, the distribution of cryoprotectant concentration is more uniform throughout the 2-mm thickness of cartilage. The 9.5-h protocol and our new 7-h protocol were tested experimentally by Wu et al. on dowels of porcine articular cartilage on bone, and both protocols were successful with average cell viabilities (normalized to a fresh control group) of 61.9 ± 11.9% (mean ± SE) and 77.7 ± 3.7%, respectively, for 10-mm diameter dowels vitrified in liquid nitrogen in 50 ml tubes and rewarmed in a 37 °C water bath [57].

3.3. Importance of nonideality for freezing point calculations

Fig. 4 illustrates the predicted freezing point throughout a 2-mm thick piece of cartilage at the end of each loading step of the new 7-h protocol when the solution is assumed to be nonideal and concentrated (Equation (7)–(9)) *vs.* ideal and dilute (Equation (13)). At the end
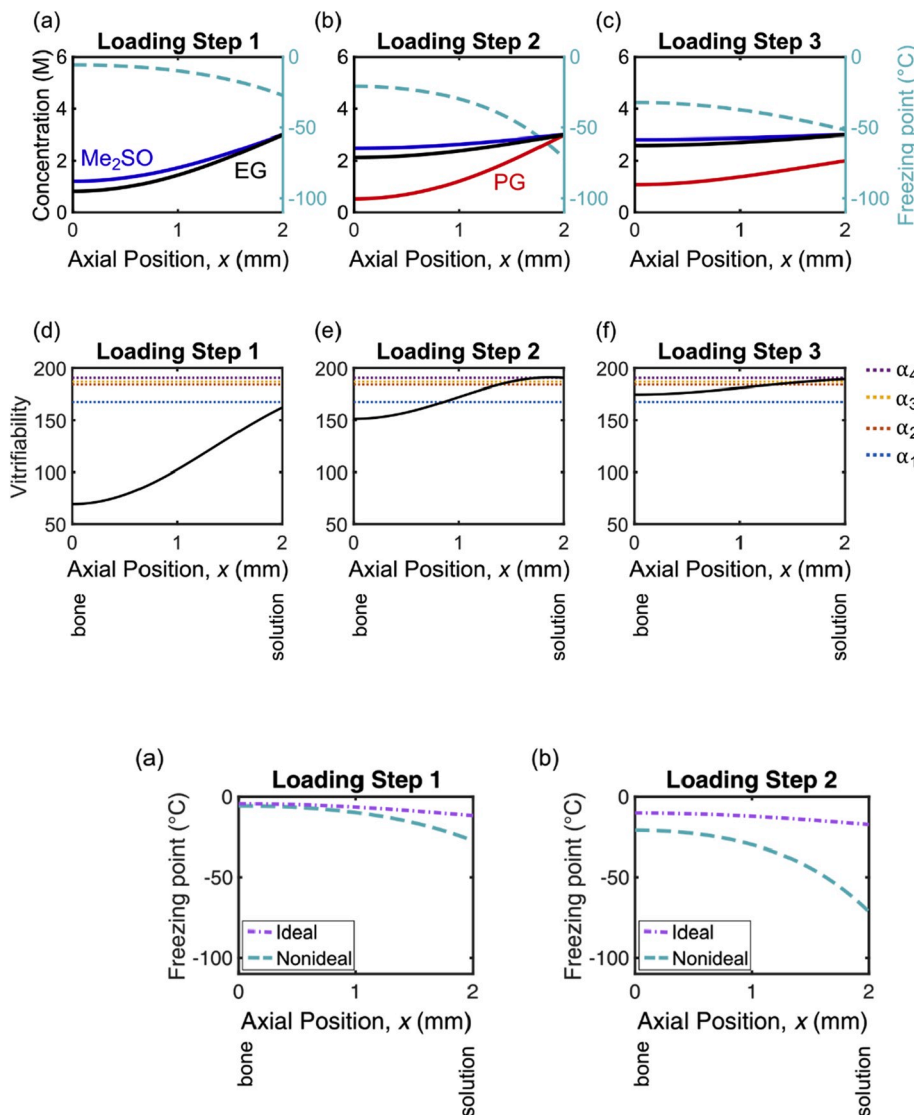
Fig. 3. (a)–(c) Spatial distribution of cryoprotectant concentration (solid lines; blue is Me₂SO, red is PG, and black is EG; left *y*-axis) and nonideal freezing point (dashed line, light blue; right *y*-axis) in a 2-mm cartilage sample at the end of each step of the new 7-h protocol, the details of which are summarized in Table 6. (d)–(f) Spatial distribution of vitrifiability (black solid line) at the end of each step with vitrifiability thresholds illustrated by dotted horizontal lines (blue is α_1, red is α_2, yellow is α_3, and purple is α_4). Concentration is calculated using Equations (1)–(5), freezing point is calculated using the nonideal equations (Equation (7)–(9)), and vitrifiability is calculated using Equation (6). (For interpretation of the references to colour in this figure legend, the reader is referred to the Web version of this article.)

Fig. 4. Distribution of freezing point throughout a 2-mm thick piece of cartilage as calculated using the ideal (Equation (13)) and nonideal (Equation (7)–(9)) solution assumptions for (a) loading step 1, (b) loading step 2, and (c) loading step 3 of the new 7-h protocol.

Table 7
Cryoprotectant concentrations, times, and temperatures for each step of a 5-h cryoprotectant loading protocol [57].

	Concentrations	Time	Temperature
Step 1	3 M Me$_2$SO 3 M EG	90 min	0 °C
Step 2	3 M Me$_2$SO 3 M EG 3 M PG	90 min	−10 °C
Step 3	3 M Me$_2$SO 3 M EG 1 M PG	130 min	−10 °C

of the first loading step, the ideal freezing point is close to the nonideal solution freezing point, particularly at the cartilage–bone junction. This means that the total cryoprotectant concentration at this location is in fact dilute enough for Equation (13) to be accurate. However, as the total cryoprotectant concentration becomes higher at locations closer to the cartilage–solution boundary at the end of the first loading step, the ideal assumption becomes increasingly inaccurate. By the end of the second and third loading steps, the freezing points calculated assuming ideal-dilute behavior are incorrect by up to 50 °C. Through these calculations, we emphasize the importance of considering the effect of nonideality to calculate the freezing points of concentrated cryoprotectant solutions when designing vitrification protocols.

3.4. Investigating a minimally vitrifiable 5-h protocol

One experimentally tested protocol loads Me$_2$SO, PG, and EG over 5 h in 3 loading steps summarized in Table 7 [57]. The concentrations, times, and temperatures of exposure were selected so that the full cartilage thickness would be on the verge of completely vitrifying. For each of the steps in this 5-h protocol, we calculate the expected spatial distribution of cryoprotectant concentration (Equation (1)–(5)), freezing point (Equation (7)–(9)), and vitrifiability (Equation (6)), as illustrated in Fig. 5. Less than half of the cartilage thickness is expected to be vitrifiable by the end of the last loading step (Fig. 5f). Experimentally, only $28.5 \pm 7.5\%$ (mean $\pm$ SE; normalized to a fresh control group) of cells were viable in 10-mm diameter dowels vitrified in liquid nitrogen

in 50 ml tubes and rewarmed in a 37 °C water bath [57], and this result can be explained by the insufficient level of vitrifiability for the majority of the cartilage thickness.

4. Conclusions

We have investigated the spatial and temporal distribution of vitrifiability as a new criterion for developing a successful vitrification protocol for the long-term storage of human articular cartilage. We calculated the vitrifiability distribution for a 9.5-h protocol previously reported to be successful [33] and confirmed that the whole thickness of a 2-mm thick cartilage sample exposed to the 9.5-h cryoprotectant loading protocol is vitrifiable by the end of the protocol. Based on the new vitrifiability criterion and a 7-h constraint on total loading time, we proposed a new 3-step protocol that loads dimethyl sulfoxide, propylene glycol, and ethylene glycol at progressively lower temperatures. This new 7-h protocol uses a final equilibration step to flatten the spatial distribution of cryoprotectant concentration and lower the toxicity experienced by cells close to the cartilage–solution boundary. To design the new 7-h protocol, calculations of CPA permeation, vitrifiability, and freezing point were used. We illustrate the importance of using non-ideal, non-dilute equations for freezing point in the design of vitrification protocols. As predicted in the present study, a separate paper reports that the new 7-h protocol was successful when performed on 10-mm diameter porcine articular cartilage dowels (cell viability of $77.7 \pm 3.7\%$ (mean $\pm$ SE; normalized to a fresh control group)) [57]. This new 7-h protocol is anticipated to facilitate the storage of articular cartilage for extended periods of time in a tissue bank for osteochondral allograft transplantation.

Author contributions

KW, LL, NMJ, and JAWE defined the clinical requirements. NS, NMJ and JAWE designed the computational study. ZC, SCY, and NS performed the computational study under the direction of JAWE. NS, ZC, SCY, NMJ, and JAWE evaluated the results. NS wrote the first draft of the manuscript. All authors contributed to, and approved, the final manuscript.
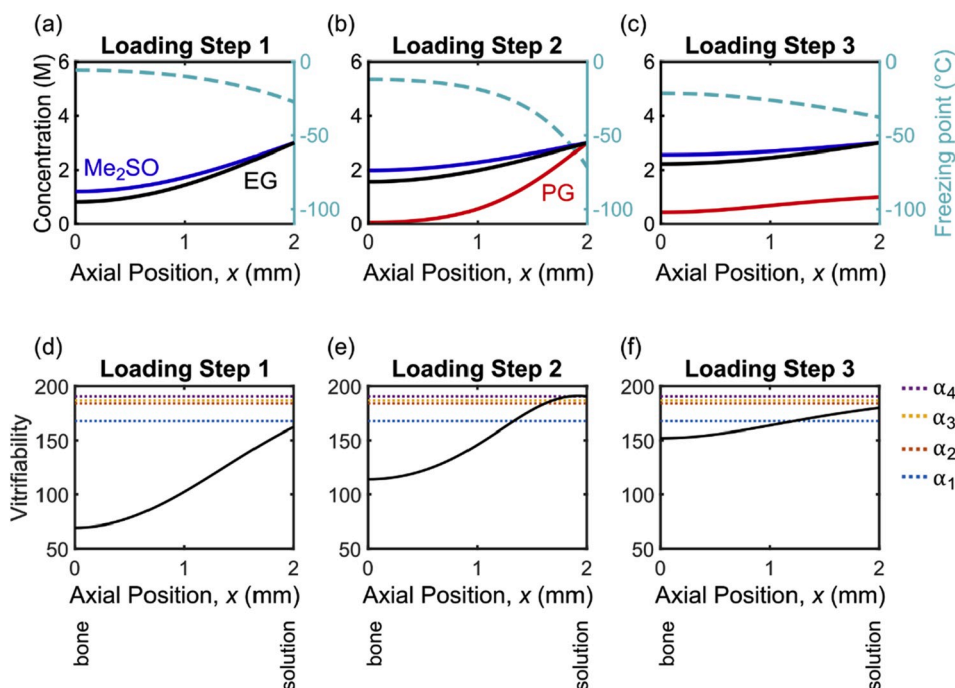
Fig. 5. (a)–(c) Spatial distribution of cryoprotectant concentration (solid lines; blue is Me$_2$SO, red is PG, and black is EG; left y-axis) and freezing point (dashed line, light blue; right y-axis) in a 2-mm cartilage sample at the end of each step of an unsuccessful 5-h protocol, the details of which are summarized in Table 7. (d)–(f) Spatial distribution of vitrifiability (black solid line) at the end of each step with vitrifiability thresholds illustrated by dotted horizontal lines (blue is α_1, red is α_2, yellow is α_3, and purple is α_4). Concentration is calculated using Equations (1)–(5), freezing point is calculated using the nonideal equations (Equation (7)–(9)), and vitrifiability is calculated using Equation (6). (For interpretation of the references to colour in this figure legend, the reader is referred to the Web version of this article.)

Declaration of competing interest

Authors NMJ and JAWE hold US Patent No. 8,758,988 & CA Patent No. 2,778,202: N.M. Jomha, L.E. McGann, J.A.W. Elliott, G. Law, F. Forbes, A. Torghabeh Abazari, B. Maghdoori and A. Weiss, "Cryopreservation of articular cartilage".

Acknowledgements

References

[1] A. Abazari, J.A.W. Elliott, G.K. Law, L.E. McGann, N.M. Jomha, A biomechanical triphasic approach to the transport of nondilute solutions in articular cartilage, Biophys. J. 97 (2009) 3054–3064.

[2] A. Abazari, J.A.W. Elliott, L.E. McGann, R.B. Thompson, MR spectroscopy measurement of the diffusion of dimethyl sulfoxide in articular cartilage and comparison to theoretical predictions, Osteoarthr. Cartil. 20 (2012) 1004–1010.

[3] A. Abazari, N.M. Jomha, J.A.W. Elliott, L.E. McGann, Review: cryopreservation of articular cartilage, Cryobiology 66 (2013) 201–209.

[4] A. Abazari, N.M. Jomha, G.K. Law, J.A.W. Elliott, L.E. McGann, Erratum to "Permeation of several cryoprotectants in porcine articular cartilage" [Cryobiology. 58 (2009) 110-114], Cryobiology 59 (2009) 369.

[5] A. Abazari, R.B. Thompson, J.A.W. Elliott, L.E. McGann, Transport phenomena in articular cartilage cryopreservation as predicted by the modified triphasic model and the effect of natural inhomogeneities, Biophys. J. 102 (2012) 1284–1293.

[6] K.A. Almansoori, V. Prasad, J.F. Forbes, G.K. Law, L.E. McGann, J.A.W. Elliott, N. M. Jomha, Cryoprotective agent toxicity interactions in human articular chondrocytes, Cryobiology 64 (2012) 185–191.

[7] S.T. Ball, D. Amiel, S.K. Williams, W. Tontz, A.C. Chen, R.L. Sah, W.D. Bugbee, The effects of storage on fresh human osteochondral allografts, Clin. Orthop. Relat. Res. 418 (2004) 246–252.

[8] J.D. Benson, A.J. Kearsley, A.Z. Higgins, Mathematical optimization of procedures for cryoprotectant equilibration using a toxicity cost function, Cryobiology 64 (2012) 144–151.

[9] B.P. Best, Cryoprotectant toxicity: facts, issues, and questions, Rejuvenation Res. 18 (2015) 422–436.

[10] K.G.M. Brockbank, Z.Z. Chen, Y.C. Song, Vitrification of porcine articular cartilage, Cryobiology 60 (2010) 217–221.

[11] W.D. Bugbee, F.R. Convery, Osteochondral allograft transplantation, Clin. Sports Med. 18 (1999) 67–75.

[12] W.D. Bugbee, A.L. Pallante-Kichura, S. Görtz, D. Amiel, R. Sah, Osteochondral allograft transplantation in cartilage repair: graft storage paradigm, translational models, and clinical applications, J. Orthop. Res. 34 (2016) 31–38.

[13] L.H. Campbell, K.G.M. Brockbank, Cryopreservation of porcine aortic heart valve leaflet-derived myofibroblasts, Biopreserv. Biobanking 8 (2010) 211–217.

[14] F. De Caro, S. Bisicchia, A. Amendola, L. Ding, Large fresh osteochondral allografts of the knee: a systematic clinical and basic science review of the literature, Arthroscopy 31 (2015) 757–765.

[15] F.R. Convery, M.H. Meyers, W.H. Akeson, Fresh osteochondral allografting of the femoral condyle, Clin. Orthop. Relat. Res. 273 (1991) 139–145.

[16] Design Institute for Physical Properties, Sponsored by AIChE, DIPPR Project 801 - Full Version, 2016.

[17] D.R. Diduch, J.N. Insall, W.N. Scott, G.R. Scuderi, D. Font-Rodriguez, Total knee replacement in young, active patients, J. Bone Jt. Surg. 79 (1997) 575–582.

[18] J.A.W. Elliott, R.C. Prickett, H.Y. Elmoazzen, K.R. Porter, L.E. McGann, A multisolute osmotic virial equation for solutions of interest in biology, J. Phys. Chem. B 111 (2007) 1775–1785.

[19] H.Y. Elmoazzen, A. Poovadan, G.K. Law, J.A.W. Elliott, L.E. McGann, N.M. Jomha, Dimethyl sulfoxide toxicity kinetics in intact articular cartilage, Cell Tissue Bank. 8 (2007) 125–133.

[20] B.C. Emmerson, S. Görtz, A.A. Jamali, C. Chung, D. Amiel, W.D. Bugbee, Fresh osteochondral allografting in the treatment of osteochondritis dissecans of the femoral condyle, Am. J. Sports Med. 35 (2007) 907–914.

[21] M.D. Fahmy, K.A. Almansoori, L. Laouar, V. Prasad, L.E. McGann, J.A.W. Elliott, N. M. Jomha, Dose–injury relationships for cryoprotective agent injury to human chondrocytes, Cryobiology 68 (2014) 50–56.

[22] G.M. Fahy, The relevance of cryoprotectant "toxicity" to cryobiology, Cryobiology 23 (1986) 1–13.

[23] G.M. Fahy, Cryoprotectant toxicity neutralization, Cryobiology 60 (2010) S45–S53.

[24] G.M. Fahy, B. Wowk, Principles of cryopreservation by vitrification, in: Cryopreservation and Freeze-Drying Protocols, Springer, New York, NY, 2015, pp. 21–82.

[25] G.M. Fahy, B. Wowk, J. Wu, S. Paynter, Improved vitrification solutions based on the predictability of vitrification solution toxicity, Cryobiology 48 (2004) 22–35.

[26] J. Farrant, Mechanism of cell damage during freezing and thawing and its prevention, Nature 205 (1965) 1284–1287.

[27] A.E. Gross, W. Kim, F. Las Heras, D. Backstein, O. Safir, K.P.H. Pritzker, Fresh osteochondral allografts for posttraumatic knee defects: long-term followup, Clin. Orthop. Relat. Res. 466 (2008) 1863–1870.

[28] A.E. Gross, N. Shasha, P. Aubin, Long-term followup of the use of fresh osteochondral allografts for posttraumatic knee defects, Clin. Orthop. Relat. Res. 435 (2005) 79–87.

[29] W.Y. Gu, W.M. Lai, V.C. Mow, A mixture theory for charged-hydrated soft tissues containing multi-electrolytes: passive transport and swelling behaviors, J. Biomech. Eng. 120 (1998) 169–180.

[30] K. Hjelle, E. Solheim, T. Strand, R. Muri, M. Brittberg, Articular cartilage defects in 1,000 knee arthroscopies, Arthroscopy 18 (2002) 730–734.

[31] E.B. Hunziker, K. Lippuner, M.J.B. Keel, N. Shintani, An educational review of cartilage repair: precepts & practice—myths & misconceptions—progress & prospects, Osteoarthr. Cartil. 23 (2015) 334–350.

[32] N.M. Jomha, P.C. Anoop, L.E. McGann, Intramatrix events during cryopreservation of porcine articular cartilage using rapid cooling, J. Orthop. Res. 22 (2004) 152–157.

[33] N.M. Jomha, J.A.W. Elliott, G.K. Law, B. Maghdoori, J. Fraser Forbes, A. Abazari, A.B. Adesida, L. Laouar, X. Zhou, L.E. McGann, Vitrification of intact human articular cartilage, Biomaterials 33 (2012) 6061–6068.

[34] N.M. Jomha, G.K. Law, A. Abazari, K. Rekieh, J.A.W. Elliott, L.E. McGann, Permeation of several cryoprotectant agents into porcine articular cartilage, Cryobiology 58 (2009) 110–114.

[35] N.M. Jomha, A.D.H. Weiss, J. Fraser Forbes, G.K. Law, J.A.W. Elliott, L.E. McGann, Cryoprotectant agent toxicity in porcine articular chondrocytes, Cryobiology 61 (2010) 297–302.

[36] J.A. Keeney, S. Eunice, G. Pashos, R.W. Wright, J.C. Clohisy, What is the evidence for total knee arthroplasty in young patients?: a systematic review of the literature, Clin. Orthop. Relat. Res. 469 (2011) 574–583.

[37] A.J. Krych, C.M. Robertson, R.J. Williams, Return to athletic activity after osteochondral allograft transplantation in the knee, Am. J. Sports Med. 40 (2012) 1053–1059.

[38] L.L. Kuleshova, S.S. Gouk, D.W. Hutmacher, Vitrification as a prospect for cryopreservation of tissue-engineered constructs, Biomaterials 28 (2007) 1585–1596.

[39] W.M. Lai, J.S. Hou, V.C. Mow, A triphasic theory for the swelling and deformation behaviors of articular cartilage, J. Biomech. Eng. 113 (1991) 245–258.

[40] A. Lawson, H. Ahmad, A. Sambanis, Cytotoxicity effects of cryoprotectants as single-component and cocktail vitrification solutions, Cryobiology 62 (2011) 115–122.

[41] A. Lawson, I.N. Mukherjee, A. Sambanis, Mathematical modeling of cryoprotectant addition and removal for the cryopreservation of engineered or natural tissues, Cryobiology 64 (2012) 1–11.

[42] M.O. Lemmon, E.W. Huber, M.L. McLinden, NIST Standard Reference Database 23: Reference Fluid Thermodynamic and Transport Properties-REFPROP, 2007.

[43] Y.D. Levy, S. Görtz, P.A. Pulido, J.C. McCauley, W.D. Bugbee, Do fresh osteochondral allografts successfully treat femoral condyle lesions? Clin. Orthop. Relat. Res. 471 (2013) 231–237.

[44] I.N. Mukherjee, Y. Li, Y.C. Song, R.C. Long, A. Sambanis, Cryoprotectant transport through articular cartilage for long-term storage: experimental and modeling studies, Osteoarthr. Cartil. 16 (2008) 1379–1386.

[45] T. Neogi, The epidemiology and impact of pain in osteoarthritis, Osteoarthr. Cartil. 21 (2013) 1145–1153.

[46] D.E. Pegg, L. Wang, D. Vaughan, Cryopreservation of articular cartilage. Part 3: the liquidus-tracking method, Cryobiology 52 (2006) 360–368.

[47] C.A. Poole, Articular cartilage chondrons: form, function and failure, J. Anat. 191 (1997) 1–13.

[48] R.C. Prickett, J.A.W. Elliott, L.E. McGann, Application of the osmotic virial equation in cryobiology, Cryobiology 60 (2010) 30–42.

[49] Z. Shaozhi, D.E. Pegg, Analysis of the permeation of cryoprotectants in cartilage, Cryobiology 54 (2007) 146–153.

[50] N. Shardt, K.K. Al-Abbasi, H. Yu, N.M. Jomha, L.E. McGann, J.A.W. Elliott, Cryoprotectant kinetic analysis of a human articular cartilage vitrification protocol, Cryobiology 73 (2016) 80–92.

[51] D.E.T. Shepherd, B.B. Seedhom, Thickness of human articular cartilage in joints of the lower limb, Ann. Rheum. Dis. 58 (1999) 27–34.

[52] S.L. Sherman, J. Garrity, K. Bauer, J. Cook, J. Stannard, W. Bugbee, Fresh osteochondral allograft transplantation for the knee: current concepts, J. Am. Acad. Orthop. Surg. 22 (2014) 121–133.

[53] Y.C. Song, F.G. Lightfoot, Z. Chen, M.J. Taylor, K.G.M. Brockbank, Vitreous preservation of rabbit articular cartilage, Cell Preserv. Technol. 2 (2004) 67–74.

[54] L. Wang, D.E. Pegg, J. Lorrison, D. Vaughan, P. Rooney, Further work on the cryopreservation of articular cartilage with particular reference to the liquidus tracking (LT) method, Cryobiology 55 (2007) 138–147.

[55] A.D.H. Weiss, J. Fraser Forbes, A. Scheuerman, G.K. Law, J.A.W. Elliott, L.E. McGann, N.M. Jomha, Statistical prediction of the vitrifiability and glass stability of multi-component cryoprotective agent solutions, Cryobiology 61 (2010) 123–127.

[56] B. Wowk, Thermodynamic aspects of vitrification, Cryobiology 60 (2010) 11–22.

[57] K. Wu, N. Shardt, L. Laouar, Z. Chen, V. Prasad, J.A.W. Elliott, N.M. Jomha, Comparison of Three Multi-Cryoprotectant Loading Protocols for Vitrification of Porcine Articular Cartilage, Submitted to Cryobiology, 2019, https://doi.org/10.1016/j.cryobiol.2020.01.001.

[58] M.W. Zielinski, L.E. McGann, J.A. Nychka, J.A.W. Elliott, Comparison of non-ideal solution theories for multi-solute solutions in cryobiology and tabulation of required coefficients, Cryobiology 69 (2014) 305–317.